

ORIGINAL RESEARCH

Estimating inundation of small waterbodies with sub-pixel analysis of Landsat imagery: long-term trends in surface water area and evaluation of common drought indices

Ibrahima Sall^{1,2}, Christopher J. Jarchow³, Brent H. Sigafus², Lisa A. Eby¹, Michael J. Forzley^{1,4} & Blake R. Hossack^{1,4} 

¹Wildlife Biology Program, W. A. Franke College of Forestry and Conservation, University of Montana, Missoula, Montana, USA

²U.S. Geological Survey, Southwest Biological Science Center, Tucson, Arizona, USA

³Biosystems Engineering, University of Arizona, Tucson, Arizona, USA

⁴U.S. Geological Survey, Northern Rocky Mountain Science Center, Missoula, Montana, USA

Keywords

Drought, Landsat, matched filtering, small waterbodies, spectral unmixing, surface water estimation

Correspondence

Blake R. Hossack, USGS Northern Rocky Mountain Science Center, Wildlife Biology Program, University of Montana, Missoula, MT. Tel: 406-243-4495; Fax: 406-243-6064; E-mail: blake_hossack@usgs.gov

Editor: Kate He

Associate Editor: András Zlinszky

Received: 20 December 2019; Revised: 14 April 2020; Accepted: 8 June 2020

doi: 10.1002/rse2.172

Abstract

Small waterbodies are numerically dominant in many landscapes and provide several important ecosystem services, but automated measurement of waterbodies smaller than a standard Landsat pixel (0.09 ha) remains challenging. To further evaluate sub-Landsat pixel techniques for estimating inundation extent of small waterbodies (basin area: 0.06–1.79 ha), we used a partial spectral unmixing method with matched filtering applied to September 1985–2018 Landsat 5 and eight imagery from southern Arizona, USA. We estimated trends in modeled surface water area each September and evaluated the ability of several common drought indices to explain variation in mean water area. Our methods accurately classified waterbodies as dry or inundated (Landsat 5: 91.3%; Landsat 8: 98.9%) and modeled and digitized surface water areas were strongly correlated ($R^2 = 0.70$ –0.92; bias = –0.024 to –0.015 ha). Estimated surface water area was best explained by the 3-month seasonal standardized precipitation index (SPI03; July–September). We found a wide range of estimated relationships between drought indices (e.g. SPI vs. Palmer Drought Severity Index) and estimated water area, even for different durations of the same drought index (e.g. SPI01 vs. SPI12). Mean waterbody surface area decreased by ~14% from September 1985 to September 2018, which matches declines in local annual precipitation and regional trends of reduced inundation extent of larger waterbodies. These results emphasize the importance of understanding local systems when relying on drought indices to infer variation in past or future surface water dynamics. Several challenges remain before widespread application of sub-pixel methods is feasible, but our results provide further evidence that partial spectral unmixing with matched filtering provides reliable measures of inundation extent of small waterbodies.

Introduction

Small waterbodies are often disproportionately important for regional biodiversity and conservation (Gibbs, 1993; Williams et al., 2003; Scheffer et al., 2006). Because of their numerical dominance across landscapes and significance for rare or imperiled species (Brooks, 2005; Downing et al., 2006), accurate and efficient measurement of hydrologic dynamics of waterbodies such as those <1 ha

is important. Accurate measurement of water resources across a landscape is also important for understanding changes in water availability over time and in response to drought (Halabisky et al., 2016; Carroll and Loboda, 2017).

There are still many significant limitations to measuring hydrologic dynamics of small waterbodies. Accurate assessment of water resources is possible if high-resolution data (e.g. ≤ 1 m) are available, but because these data

are often expensive and restricted in geographic and temporal scope, there is limited ability to monitor small waterbodies over time (Tiner, 1990; Gallant, 2015). In contrast, the Landsat suite of satellites provides >30 years of imagery collected every 16 days that can be used to measure and track long-term hydrologic dynamics globally, with the important trade-off that the resulting imagery is collected at a resolution of 30 m (e.g. Pekel et al., 2016).

While error from using 30-m resolution imagery might be insignificant for measuring hydrologic dynamics of large waterbodies, the same absolute error applied to small waterbodies – especially those smaller than a single Landsat pixel (0.09 ha) – could preclude accurate determination of the presence of water, let alone measuring the amount of water. For example, in a case study from the Canadian arctic, sites ≤ 0.1 ha represented 37% of all waterbodies on the landscape and were the most susceptible to shrinking or drying, but standard methods applied to Landsat data could not be used to monitor the dynamics of waterbodies once they were <0.09 ha (Carroll and Loboda, 2017). Limitations on measuring small waterbodies, as in Carroll and Loboda (2017), can greatly hinder our ability to estimate and understand system dynamics. More recent satellite missions such as the European Space Agency's Sentinel-2A and -2B provide higher temporal (5-d combined) and spatial resolution (10 m) alternatives to Landsat, but lack the historic record needed to track long-term hydrologic dynamics.

Many methods are used to measure hydrologic variation in waterbodies smaller than a single Landsat pixel (i.e. sub-pixel methods), including regression trees (Rover et al., 2010; Huang et al., 2014; Jin et al., 2017), discrete particle swarm optimization (Li et al., 2015), Dynamic Surface Water Extent (DeVries et al., 2017; Jones, 2019), and spectral unmixing methods (Halabisky et al., 2016; Liu et al., 2017; Bishop-Taylor et al., 2019; Hong et al., 2019). Linear spectral mixture analysis, a spectral unmixing technique, estimates the relative abundance of individual components (spectral endmembers) on a pixel-by-pixel basis based on their unique spectral characteristics (Hu et al., 1999; Heinz and Chang, 2001), so fractional abundances can be converted to surface areas (Halabisky et al., 2016). While full linear spectral unmixing requires all the relevant endmember spectral inputs within an image scene to be identified and selected, partial unmixing, such as matched filtering, requires only a single target endmember (Frohn et al., 2012; Jarchow et al., 2019). Recently, Jarchow et al. (2019) compared the ability of partial (matched filtering) and full linear spectral mixture analysis methods to estimate size of small waterbodies in southern Arizona, USA, and northern Sonora, Mexico. They found extent of water estimated via matched

filtering was similar or even more accurate than estimates from linear spectral mixture analysis, despite the method being simpler and requiring fewer spectral inputs, but they applied it to a limited Landsat record.

Many organisms use or are even limited to small waterbodies, so it is important to be able to measure the hydrologic variability and drought sensitivity of these habitats efficiently and accurately. In south-western North America, imperiled taxa, such as the Chiricahua leopard frog (*Rana chiricahuensis*) and, especially, the Sonoran tiger salamander (*Ambystoma mavortium stebbinsi*), now rely primarily upon small waterbodies (Jarchow et al., 2016; Hossack et al., 2017). Now rare compared to human-created ponds, small, natural wetlands in the Southwest also host a disproportionate number of imperiled aquatic species such as fishes, invertebrates, and plants (Minckley et al., 2013). Drying of waterbodies during drought can cause mortality of aquatic organisms directly, or indirectly by increased predation and disease transmission as waterbodies shrink (Greer and Collins, 2008; Rehage et al., 2014). Drought indices are often used to infer past habitat conditions for aquatic and semi-aquatic species (Lake, 2003; Hossack et al., 2013; Walls et al., 2013), but there has been comparatively little evaluation of their ability to describe hydrologic dynamics of small or shallow waterbodies (Zhao et al., 2017; Davis et al., 2019).

To more accurately measure the extent of small waterbodies (basin area: 0.06–1.79 ha) and evaluate broad-scale changes in water extent (water area: 0.00–1.61 ha) over time, we further refined and applied methods developed by Jarchow et al. (2019) to Landsat imagery of the San Rafael Valley (Arizona, USA). We used inundation extent of waterbodies estimated with matched filtering methods to estimate changes in the amount of water on the landscape during September 1985–2018. We then used those estimates to evaluate the performance of several common drought indices, based on data inputs from 1 to 24 months, and to determine how well they explained variation in water extent and drying and flooding dynamics.

Materials and Methods

Study area

Our study area included the San Rafael Valley and neighboring areas in southern Arizona (Fig. 1). The study area ranged from ~1400 to ~1500 m in elevation and is predominately flat grassland, transitioning into riparian deciduous and Madrean evergreen woodland near the surrounding mountains. Annual precipitation averages ~438 mm, with the majority (~270 mm) of rainfall

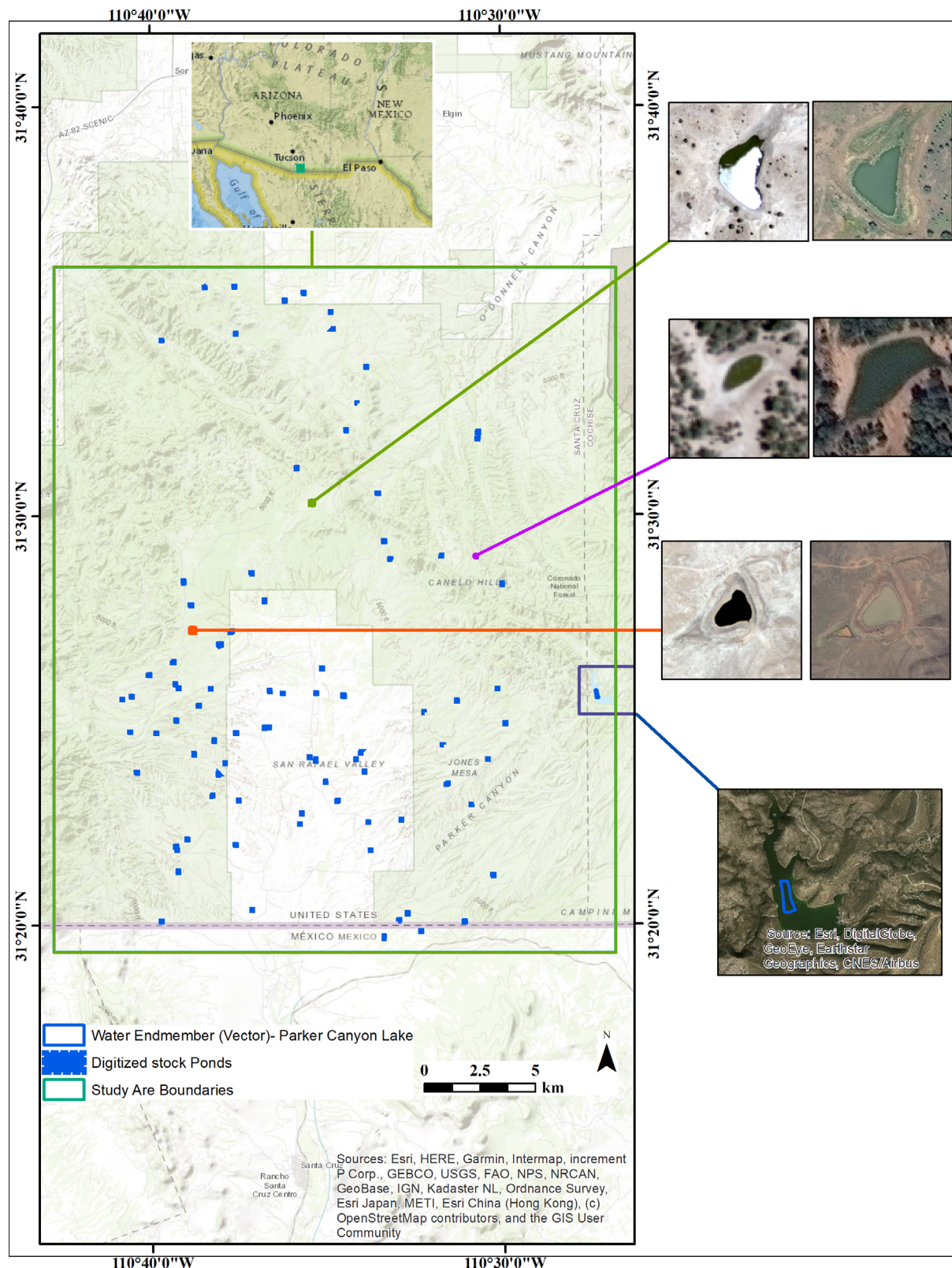


Figure 1. Study area in southern Arizona (USA) showing water endmember location (Parker Canyon Lake; bottom right) and examples of three waterbodies with different sizes and spectral characteristics using June 2007 Landsat 5 TM (left) and September 2018 Landsat 8 OLI (right).

occurring during the summer rainy (monsoon) season (ADWR, 2014).

Most surface waters in the study area are now human-created ponds built for livestock. These ponds capture runoff during rain events and are typically isolated from one another. Water storage and retention vary widely among ponds, with some holding water year-round and others holding water only intermittently. Many ponds also have wells that reduce variation in water levels and ensure water is present year-round.

Landsat imagery

Our study area fell within two Landsat scenes (path 35, row 38 and path 36, row 38). All downloaded images were processed as Tier 1 Level 1 terrain-corrected products and retrieved from Earth Explorer (<https://earthexplorer.usgs.gov>). Our search was restricted to images with <20% cloud cover taken during September 1985–2018 and returned 81 images (67 Landsat 5 and 14 Landsat 8 scenes) that we clipped to the shapefile of our study area. We used September data because it followed the summer storm season that fills small waterbodies.

Some Landsat scenes (path 36, row 38) did not cover the entire study area. Therefore, we considered only 41 images covering all ponds in the study area. Each image was visually assessed for quality and only 39 cloud-free images covering the digitized ponds in the study area were chosen for further processing. Because of spatial and spectral resolution consistency requirements between platforms to perform our analyses, we only considered six individual bands (blue, green, red, near infrared [NIR], short-wave infrared [SWIR] 1, and SWIR 2; Fig. 2A) and created a composite image for our study area (Halabisky et al., 2016; Jarchow et al., 2019). See Figure 3 for a summary of procedures we used to process imagery.

Reference data

For validation, we used high-resolution satellite imagery from DigitalGlobe WorldView-2 and National Agriculture Imagery Program (NAIP) that had the closest dates to the selected Landsat images. For Landsat 5, we used a 1-m NAIP image obtained on 25 June 2007 to validate the Landsat image acquired on 27 June 2007. A WorldView-2 image with a resolution of 0.46 m and acquired on 27

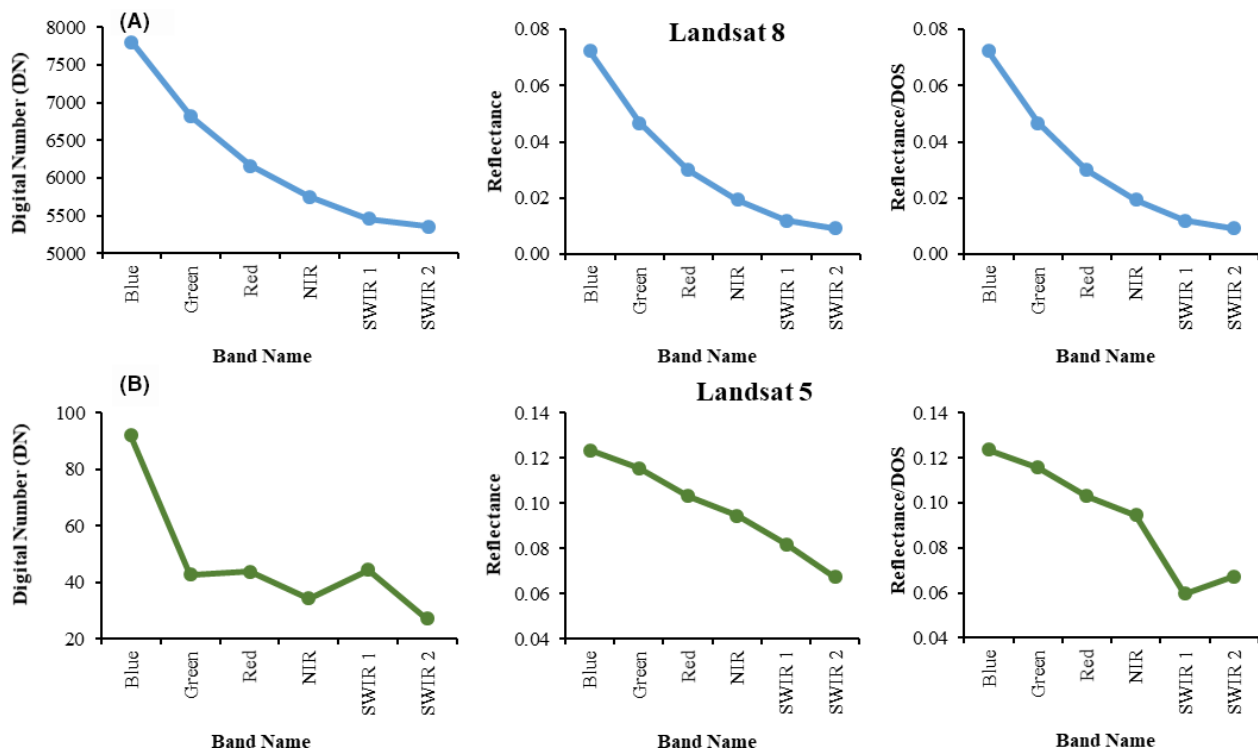


Figure 2. Spectral signature curves of water endmember extracted from Landsat imagery validation dates with, respectively from left to right, raw data (digital number [DN]) and atmospheric correction (reflectance without and with dark object subtraction [DOS] correction). (A) for Landsat 8 on 29 September 2018 and (B) for Landsat 5 on 27 June 2007. Values for each of the six individual bands (blue, green, red, near infrared [NIR], short-wave infrared [SWIR] 1, and SWIR 2) are shown.

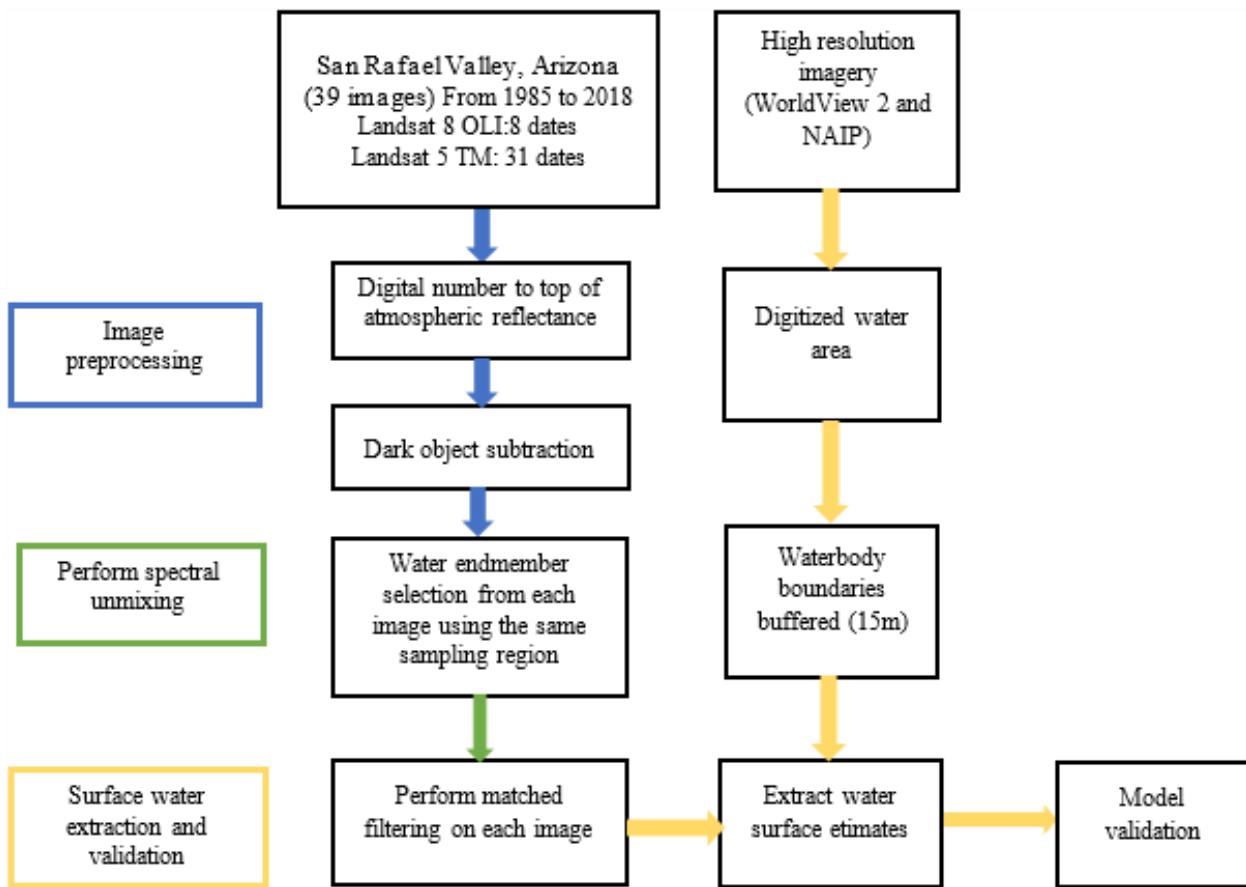


Figure 3. Procedures used to perform the partial spectral unmixing (matched filtering) in ENVI 5.2 and validation of surface water estimates in ArcGIS 10.6.

September 2018 was used to validate the Landsat 8 image obtained on 29 September 2018 (Appendix, Table S1).

Surface water delineation and validation

Using ArcGIS v10.6 and the high-resolution satellite validation imagery from DigitalGlobe WorldView-2 (0.46-m resolution) and NAIP (1-m resolution), we selected and digitized the high-water line (maximum inundation extent) of 96 waterbodies with basin dimensions that ranged from 0.06 ha to 1.79 ha. The high-water line was distinguished based on a distinct line of woody vegetation or change in soil color along the perimeter of each waterbody. When water was present, we also digitized the perimeter of the inundation extent of each waterbody to validate the Landsat 5 and Landsat 8 images. Several sites were removed from the analysis because we could not confidently determine if they were dry or wet. Using Landsat 8, 89 sites with water extents ranging from 0.02 ha to 0.34 ha were used for further analyses. Only 46 sites were selected based on the Landsat 5 image, with

water extents that ranged from 0.01 ha to 0.61 ha (Appendix, Table S1).

Precipitation and drought indices

We calculated annual precipitation totals (October–September water year) for the centroid of the study area ($\sim 783 \text{ km}^2$) from estimated monthly precipitation totals (Fig. 4; 4-km grid; <http://prism.oregonstate.edu>; accessed 31 October 2019) (Daly et al., 2008). We used four drought indices based on Palmer methods (PDSI, PHDI, ZNDX, and PMDI) and two multi-scalar drought indices (SPI and SPEI; see Table 1 for index definitions and details). For SPI and SPEI, we evaluated time scales of 1, 3, 9, 12, and 24 months to determine which time periods were most useful for describing hydrologic variability of small waterbodies in the study area. We downloaded September 1985–2018 drought indices from the National Oceanic and Atmospheric Administration for Santa Cruz County, Arizona, climate division 7 (NOAA's Gridded Climate Divisional Dataset 2015; Vose et al., 2014). The

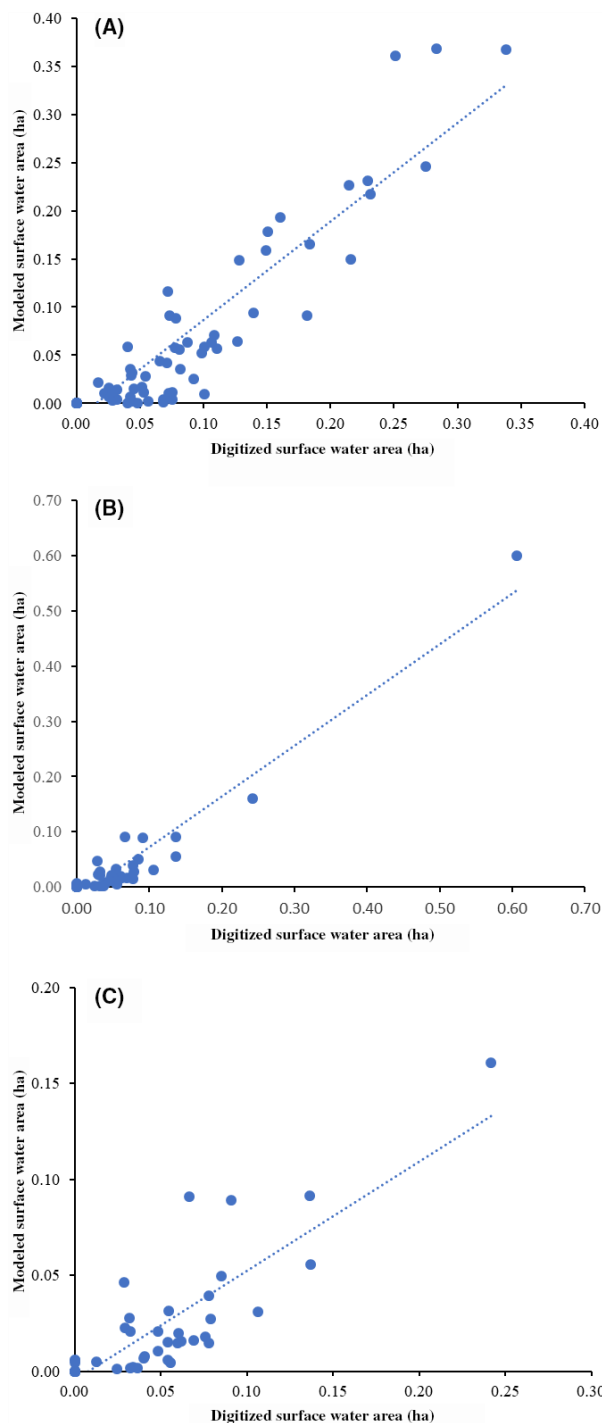


Figure 4. Estimated annual rainfall in the San Rafael Valley, Arizona, October–September 1984–2018. Rainfall declined by an average of 4.83 mm per year (linear regression: coefficient = -4.83 [$\text{SE} = 1.99$]) during the study.

SPEI data were downloaded from the SPEI Global Drought Monitor website (<https://spei.csic.es/map/maps>.

html, accessed 02 September 2019) using the shapefile of our study area as a region.

Data preprocessing and spectral unmixing analysis

We used ENVI 5.2 software (Exelis Visual Information Solutions, 2015) to process data and perform partial unmixing analysis with matched filtering. Based on composite images generated from six bands (blue, green, red, near infrared [NIR], short-wave infrared [SWIR] 1, and SWIR 2; Fig. 2), we used the radiometric correction option in ENVI to convert optical bands from digital numbers to top-of-atmosphere reflectance (Tulbure and Broich, 2013). We then used the band minimum option in dark object subtraction, an image-based atmospheric correction tool, to remove the potential effects of atmospheric scattering derived from the reflectance of dark objects and the water surface (Gilmore et al., 2015; Moses et al., 2017). Dark object subtraction applied to our Landsat validation dates changed the mean spectral signature of the SWIR 1 band for Landsat 5 but not Landsat 8 (Fig. 2B). Adding the dark object subtraction did not affect results compared to using only top-of-atmosphere reflectance correction. With the matched filtering method, we used only one endmember (water) because the technique maximizes the responses of the target endmember and matches its signature by suppressing the response of the composite unknown background of all other end-members. This method allows rapid detection of water presence and does not require knowledge of other end-members within the scene.

We were unable to extract water endmembers directly from the waterbodies because of their small inundation extents (Jarchow et al., 2019). To overcome this limitation, we extracted water endmembers from Parker Canyon Lake (Fig. 1), the closest large waterbody to our study area. To account for the best and closest spectral signatures to capture and detect waterbodies, especially for depth and water color, we extracted the mean water endmember from 53 pure water pixels. The water endmember was extracted directly from each image. We used the same sampling region (Fig. 1) for each of the 39 images, including both validation images, to perform matched filtering. Raster images generated from the matched filtering represent the fraction of water content on a per-pixel basis. Values ranged from negative to ≥ 1.0 , where negative values indicate the non-presence of water in a cell and positive values represent per cent of a cell covered by water. Values ≥ 1.0 indicated the cell was 100% covered by water.

Table 1. Description of the seven common drought indices that we used to model annual variation (September 1985–2018) in inundation extent of small waterbodies (basin area: 0.064–1.791 ha) in the San Rafael Valley, Arizona, USA.

Drought index	Description	References
Palmer drought severity index (PDSI)	Reflects meteorological drought, based on precipitation, evapotranspiration, and soil-moisture conditions	Alley, 1984; Palmer, 1965
Palmer Z index (ZNDX)	The “Moisture Anomaly Index”, reflects monthly deviations from the long-term record for a site. Derived from PDSI	Sakamoto, 1978; Karl, 1986
Palmer modified drought index (PMDI)	Weighted average of inputs used for PDSI	Heddinghaus and Sabol, 1991
Palmer Hydrological Drought Index (PHDI)	Based on PDSI, modified to reflect longer-term dryness that will affect surface and groundwater	Palmer, 1965; Karl, 1986
Standardized precipitation index (SPI)	Based on historical precipitation information, calculated over 1- to >48-month time scales	Guttman, 1998
Standardized precipitation evapotranspiration index (SPEI)	Similar to SPI but includes the role of temperature in evaporation	Vicente-Serrano et al., 2010

Surface water estimation and validation

We used rasters of surface water area estimated from the matched filtering in ArcGIS 10.6 and the waterbodies for each Landsat image validation date to assess the accuracy of these techniques for estimating surface water area (inundation extent) for the two Landsat dates (Halabisky et al., 2016; Jarchow et al., 2019). To account for small pixel shifts between images, presence of sediment traps near many waterbodies, and to avoid double counting the actual surface water area when there were neighboring ponds, we buffered the waterbodies by 15 m. Sediment traps often fill with water shortly after rain events, but they are not designed to store water and we thus did not digitize their boundaries. To estimate inundation extent, we used raster calculator in ArcGIS 10.6 to replace the negative values by zero and all values ≥ 1.0 with one. To calculate the inundation extent area of each pixel, we multiplied each cell by 900 m^2 . We generated 39 raster images with cell values ranging from 0 to 900 m^2 . Using the “spatial analyst tools” in ArcGIS 10.6 (specifically the option called “zonal statistics as table” in ArcGIS), we estimated inundation extent by summing the area of water for all cells falling within the 15-m buffered boundary (high-water lines) of each of the 89 waterbodies for 39 image dates.

To validate our matched filtering model, we used the Landsat 8 image captured on 29 September 2018 and the Landsat 5 image of 27 June 2007. For each of the validation dates, we compared the modeled surface water area to the inundation area digitized for each stock pond. Because we were not able to find high-resolution validation imagery captured within 3 days of the 39 September images captured during 1985–2018, we could not evaluate the accuracy of extracted surface water areas estimated with the matched filtering method for all dates. Therefore,

no specific validation was applied to the time series Landsat imagery (1985–2018).

Model and statistical estimations

We used estimated inundation extents for each of the 89 waterbodies to investigate their annual variation over time in the study area and to analyze the performance of commonly used drought indices with different durations (e.g. 1 mo. vs. 9 mo.). We used generalized linear mixed-effects models (*lme4* in R v 3.6.1) (Bates et al., 2015) to estimate trends in the relationship between estimated surface area of waterbodies measured over time (year, standardized) and relative to the six drought indices. We fit models to the Gamma distribution (\log_e link) using maximum likelihood methods because the response data were strongly skewed toward small values. Models fitted to the Gamma distribution cannot have zero values, so we added 0.001 ha to each measure of water surface area.

We evaluated competing mixed-effects models in two analyses. First, we fit 14 models using the full dataset of 89 waterbodies. Second, to partially account for the disproportionate effects of one very large (>0.4 ha) waterbody, we fit an identical set of 14 models but restricted the dataset to the 75 waterbodies with a maximum area extent of ≤ 0.4 ha. For both analyses, we ranked models by differences in their Akaike Information Criterion (ΔAIC), to select the top-ranked models for each set of candidate models. Although we drew most inferences from the top-ranked model for each model set, we plotted the predicted amount of water from 1985 to 2018 based on the estimated relationship between inundation extent and the different drought metrics and durations (e.g. 1 mo. vs. 9 mo.).

Wells make sites less responsive to drought conditions. We could not include the presence of wells as a covariate

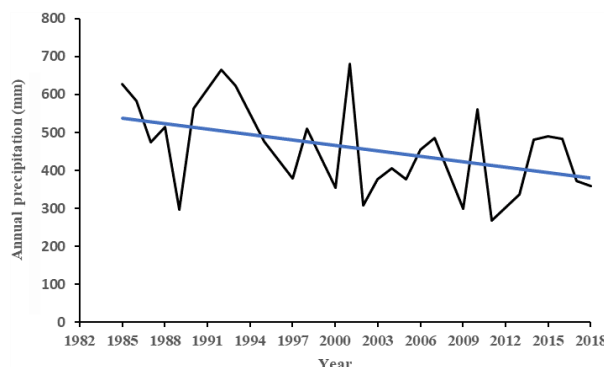


Figure 5. Comparison of digitized and estimated (matched filtering) results when (A) 89 waterbodies are included using Landsat 8 captured on 29 September 2018; (B) Landsat 5 captured on 27 June 2007 used with all digitized waterbodies (46); (C) and only 45 waterbodies from the 27 June 2007 Landsat 5 image with digitized surface water extents ≤ 0.4 ha.

because much of the valley is private and complete information on wells is unavailable. To partially account for the presence of wells on some waterbodies, we performed a post hoc analysis and fitted an identical set of 14 candidate models to only the 25 waterbodies with the most variable hydrology. We used the coefficient of variation for each site based on yearly values of September inundation extent to identify the 25 waterbodies with the most variable hydrology.

Results

Validation water surface estimations

Our results showed a strong and positive correlation between modeled surface water and digitized surface water based on Landsat 8 for the full dataset of 89 waterbodies ($b_0 = -0.016$ [SE = 0.005], $b_{\text{modeled}} = 1.024$ [SE = 0.045]; $R^2 = 0.86$; bias = -0.015; Figure 5A [bias = mean prediction error]). There was also a strong and similar relationship between modeled and digitized surface water areas based on Landsat 5 imagery ($n = 46$, $b_0 = -0.019$ [SE = 0.004], $b_{\text{modeled}} = 0.920$ [SE = 0.041]; $R^2 = 0.92$; bias = -0.024; Fig. 5B). When we excluded the one waterbody > 0.4 ha from this latter model, the strength of the relationship was weakened ($b_0 = -0.005$ [SE = 0.004], $b_{\text{modeled}} = 0.570$ [SE = 0.056]; $R^2 = 0.70$), but bias was unchanged (bias = -0.024; Fig. 5C).

Accuracy of classifying waterbodies as either dry or inundated based on comparison of digitized and modeled estimates was 98.88% (88 of 89) for Landsat 8 and 91.3% (42 of 46) for Landsat 5. For Landsat 8, 1.69% (1 of 59) digitized inundated waterbodies were misclassified as being dry and 100% (30 of 30) of dry sites were

accurately classified. While 100% (33 of 33) of digitized inundated waterbodies using Landsat 5 were accurately classified as having water, the model over-predicted the number of inundated waterbodies: 30.77% (4 of 13) waterbodies predicted to be inundated were dry. However, the highest over-predicted inundation area was 0.006 ha with a per cent of the total estimated waterbody area ranging from 0.26% to 7.27%. Those values were not substantial given that the misclassified dry areas ranged from 0.08 to 0.28 ha.

Drought effects and changes over time

Models based on 3-month seasonal standardized precipitation index (SPI03) that incorporated information for July–September were the best-supported for the datasets of all 89 waterbodies (Table 2; Fig. 6A), the 75 waterbodies with maximum area extent ≤ 0.4 ha (Table 3; Fig. 6B), and the 25 waterbodies with the most variable hydrology ($\Delta\text{AIC} = 3.58$, Fig. 7A). Drought coefficients were positive for all models (Tables 2 and 3), as expected, which indicates that increasing levels of moisture were associated with greater mean surface water in a given year. However, the effect sizes were largest for indices based on between 3 and 9 months of information (e.g. SPEI03 and SPI09). The drought effect in the top-ranked models (log_e-scale: $b_{\text{SPI03}} = 0.21$; Tables 2 and 3) was also equal for the datasets based on 89 and 75 waterbodies, which indicates that the inclusion of sites > 0.4 ha did not affect this estimated relationship.

Estimated directions and rates of change in mean surface water area varied among models. For all 89 waterbodies and the 75 waterbodies ≤ 0.4 ha, most models estimated an increase in surface water between 1988 and 2018, but the top-ranked model estimated a decline (Tables 2 and 3, Figs. 4 and 8), similar to the trend of a 4.83-mm reduction (linear regression: $b_{\text{year}} = -4.83$ [SE = 1.99]) in annual October–September rainfall for the same time period. Based on the top-ranked SPI03 models, mean surface area of waterbodies declined by ~14% from September 1985 to September 2018 for both the full dataset of 89 waterbodies and the 75 waterbodies ≤ 0.4 ha (Table 4).

The 3-month SPI model also provided the best fit for the dataset limited to the 25 waterbodies with the most variable hydrology. All models estimated a mean decrease in surface water area over time for these 25 waterbodies (range [log_e-scale]: -2.00 to -0.12) (Fig. 7B). Changes in size over time did not differ from zero (log_e-scale: $b_{\text{year}} = -1.20$ [SE = 0.75]), but this was partly due to the small sample size compared to analyses based on 89 and 75 waterbodies. Based on the top-ranked SPI03 model, the estimated ~13% net reduction in mean size of these

Table 2. Coefficients (se) from generalized linear mixed-effects models (Gamma distribution, \log_e link) that estimated the relationship between surface area of all waterbodies ($N = 89$) during September 1985–2018 in relation to common drought indices and time.

All Waterbodies					
Drought index	Intercept	Drought	Year	logLik	ΔAIC
SPI03	-2.65 (0.09)	0.21 (0.01)	-2.44 (0.70)	6044.18	0.00
SPEI03	-2.60 (0.09)	0.21 (0.01)	0.74 (0.70)	6016.53	55.31
SPI09	-2.65 (0.09)	0.19 (0.02)	2.10 (0.71)	6008.84	70.69
PMDI	-2.61 (0.09)	0.07 (0.01)	2.77 (0.73)	5990.39	107.59
SPEI09	-2.56 (0.09)	0.19 (0.01)	3.31 (0.75)	5988.10	112.17
SPI12	-2.64 (0.09)	0.13 (0.01)	2.52 (0.75)	5958.71	170.94
PHDI	-2.61 (0.09)	0.05 (0.01)	3.80 (0.80)	5954.08	180.20
PDSI	-2.59 (0.09)	0.05 (0.01)	1.76 (0.73)	5953.24	181.88
SPEI12	-2.58 (0.09)	0.15 (0.01)	3.48 (0.80)	5953.12	182.13
SPI24	-2.64 (0.09)	0.12 (0.01)	2.77 (0.79)	5939.71	208.93
ZNDX	-2.63 (0.09)	0.06 (0.01)	-2.47 (0.73)	5939.52	209.32
SPEI01	-2.64 (0.09)	0.09 (0.01)	-1.00 (0.70)	5930.29	227.78
SPI01	-2.65 (0.09)	0.10 (0.01)	-2.41 (0.75)	5927.55	233.27
SPEI24	-2.60 (0.09)	0.07 (0.01)	2.01 (0.84)	5916.20	255.96

The number after the drought metric acronym reflects the months of information included in the metric. Year was standardized prior to analysis. Models are ranked according to their log-likelihood and differences in Akaike Information Criterion (ΔAIC).

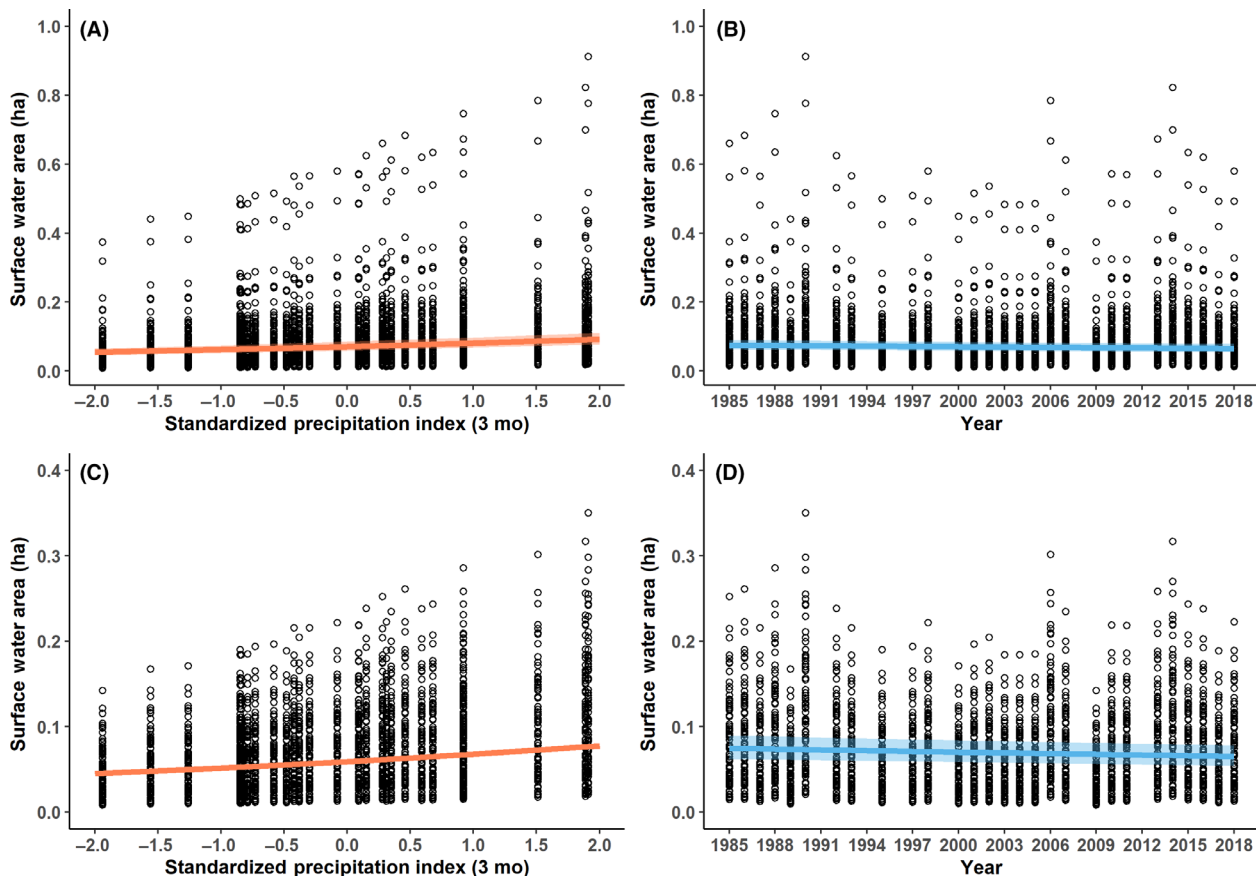


Figure 6. Estimated trends (mean \pm 95% CI) in September surface water area relative to drought (SPI03; orange line in A and C) and time (blue line in B and D), based on the full dataset of 89 waterbodies (top) and the dataset based on 75 waterbodies ≤ 0.4 ha (bottom).

Table 3. Coefficients (se) from generalized linear mixed-effects models (Gamma distribution, \log_e link) that estimated the relationship between surface area of waterbodies $\leq 0.4 \text{ ha}$ ($N = 75$) during September 1985–2018 in relation to common drought indices and time.

Waterbodies $\leq 0.4 \text{ ha}$					
Drought index	Intercept	Drought	Year	logLik	ΔAIC
SPI03	-2.83 (0.01)	0.21 (0.06)	-2.15 (0.01)	5675.19	0.00
SPEI03	-2.78 (0.07)	0.21 (0.02)	0.88 (0.79)	5649.91	50.55
SPI09	-2.83 (0.01)	0.19 (0.01)	2.04 (0.01)	5636.72	76.93
PMDI	-2.79 (0.09)	0.07 (0.01)	2.74 (0.74)	5624.59	101.20
SPEI09	-2.74 (0.01)	0.19 (0.01)	3.26 (0.01)	5621.97	106.45
SPI12	-2.82 (0.09)	0.13 (0.01)	2.52 (0.74)	5596.41	157.56
PDSI	-2.78 (0.09)	0.05 (0.01)	1.80 (0.72)	5593.03	164.31
PHDI	-2.79 (0.09)	0.05 (0.01)	3.64 (0.79)	5591.14	168.10
SPEI12	-2.76 (0.08)	0.15 (0.02)	3.38 (0.79)	5590.31	169.77
ZNDX	-2.82 (0.09)	0.06 (0.01)	-2.20 (0.72)	5580.52	189.34
SPI24	-2.82 (0.09)	0.12 (0.02)	2.73 (0.78)	5578.98	192.41
SPI01	-2.83 (0.09)	0.10 (0.01)	-2.16 (0.74)	5575.79	198.80
SPEI01	-2.82 (0.09)	0.09 (0.01)	-0.83 (0.69)	5570.05	210.29
SPEI24	-2.78 (0.09)	0.08 (0.02)	2.03 (0.83)	5558.78	232.82

The number after the drought metric acronym reflects the months of information included in the metric. Year was standardized prior to analysis. Models are ranked according to their log-likelihood and differences in Akaike Information Criterion (ΔAIC).

waterbodies was similar to that of the larger datasets (Table 4).

Discussion

We applied a partial spectral unmixing method (matched filtering) to 30-m Landsat 5 and Landsat 8 imagery to predict the inundation extent of waterbodies with a broad range of spectral characteristics (e.g. algal or turbid; Fig. 9) and sizes (basin area: 0.064–1.791 ha; Fig. 10) in southern Arizona, USA. Sub-pixel methods are important for monitoring water resources and dynamics of small waterbodies that dominate many landscapes but still pose problems for efficient, large-scale estimation from publicly available data (Rover et al., 2010; Li et al., 2015; Carroll and Loboda, 2017). Our model capably predicted inundation extent, allowing us to estimate trends in surface water extent for the 34-year Landsat record and to assess the relationship with common drought indices. Our results provide further evidence that partial spectral unmixing (matched filtering) methods provide reliable measures of inundation extent of waterbodies, including those smaller than a Landsat pixel.

The relationship between modeled and digitized surface water in our study was strong for both the Landsat 8 ($R^2 = 0.86$, bias = -0.015) and Landsat 5 ($R^2 = 0.70$ –0.92; bias = -0.024) datasets. The refinements (e.g. dark object subtraction) we made to the methods in Jarchow et al. (2019) suggest an increase in classification accuracy with similar, small bias. Although many complex

atmospheric correction routines are available, some of these methods, including stock Landsat 8 Surface Reflectance Code and Landsat Ecosystem Disturbance Adaptive Processing System, have performed poorly for small, spectrally altered waterbodies (Torbick et al., 2013; Ilori et al., 2019). Jarchow et al. (2019), who also applied matched filtering to the San Rafael Valley, AZ, reported poorer performance of these Landsat products compared to raw digital numbers. However, top-of-atmosphere reflectance correction used in our current study may have improved performance of our spectral unmixing model and could be an effective alternative to more complex routines.

Several challenges remain for widespread application of sub-pixel methods to small waterbodies. These challenges include turbid, green, or brown appearance, and the irregular shape of many small waterbodies. Because of high edge-to-area ratios for small sites, estimation error caused by irregular shapes is magnified compared to large sites. Waters with unusual colors are common in the Southwest and many other areas, often in response to storms, livestock use, or seasonal algal blooms (Figs. 1 and 9; Canals et al., 2011; Jarchow et al., 2019). The high turbidity of many waterbodies in our study area made it difficult to determine from reference images whether some waterbodies were dry or inundated, and removing some sites due to uncertainty about their inundation status might have artificially improved model performance. Based on the validation datasets, our methods tended to slightly overestimate the inundation extent of waterbodies (Fig. 5), possibly because of the presence of sediment

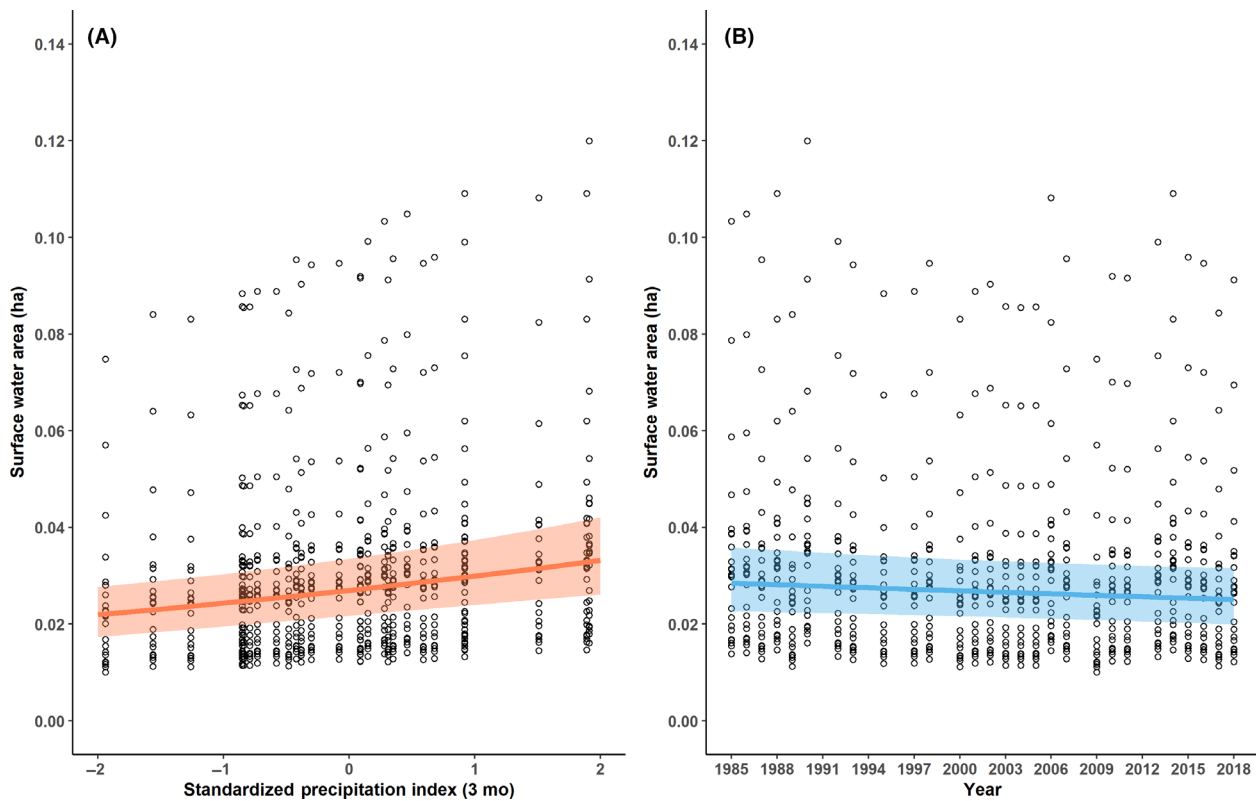


Figure 7. Estimated trend ($\text{mean} \pm 95\% \text{ CI}$) in September surface water area relative to drought (A) and time (B), based on the 25 waterbodies with the most variable hydrology.

traps that are designed to temporarily retain excess water. However, our results do not suggest that the misclassifications were related to basin size or spectral characteristics of waterbodies, and our estimates from the 1985–2018 dataset were consistent whether we included all waterbodies or only those $\leq 0.4 \text{ ha}$.

Application of our estimation methods to September 1985–2018 Landsat imagery revealed large variation in the relationships between drought indices and estimated surface water, similar to the large range of correlation coefficients among drought indices and durations (Appendix, Table S2). Coefficients for drought indices in the fitted models were always positive, as expected, because positive values of drought indices represent above-average moisture conditions. But based on analysis of all 89 waterbodies or only the 75 waterbodies $\leq 0.4 \text{ ha}$, coefficients ranged from 0.06 (log_e-scale) for PDSI and PHDI to 0.25 (log_e-scale) for the top-ranked SPI03 model (Tables 2 and 3). The drought indices PHDI, PMDI, and ZNDX, which are often used to model variation in dynamics of small waterbodies (e.g. Hossack et al., 2013; Walls et al., 2013), were only weakly related to September water conditions and performed poorly compared to simple indices like SPI for our study area. Similar to our study, SPI best described

dynamics of vernal pools in the north-east USA and montane wetlands in California (Davis et al., 2019).

We expected SPEI to out-perform SPI in our hot, arid study area because SPEI is based on SPI but incorporates the added effect of temperature on evaporation and drought (Vicente-Serrano et al., 2010). In a global assessment of drought indices to reflect agricultural, hydrological, and ecological responses to drought, SPI and SPEI performed similarly, except SPEI better represented responses to drought during summer (Vicente-Serrano et al., 2012). For our analyses, the simpler SPI was always better supported for a given time period than SPEI except for one of the models based on 1 month of information. It is possible that SPEI might have performed better if we had modeled water area during hotter, drier times of the year, such as June.

Our September measurements of water area occurred after the wettest season of the year in the Southwest (Adams and Comrie, 1997) and most of our sites fill from storm runoff rather than interactions with groundwater. Accordingly, in all of our analyses, model rankings were generally inversely related to the duration of the drought metric, except for those based on only 1 month of data. That is, 3-month indices had the largest effect sizes,

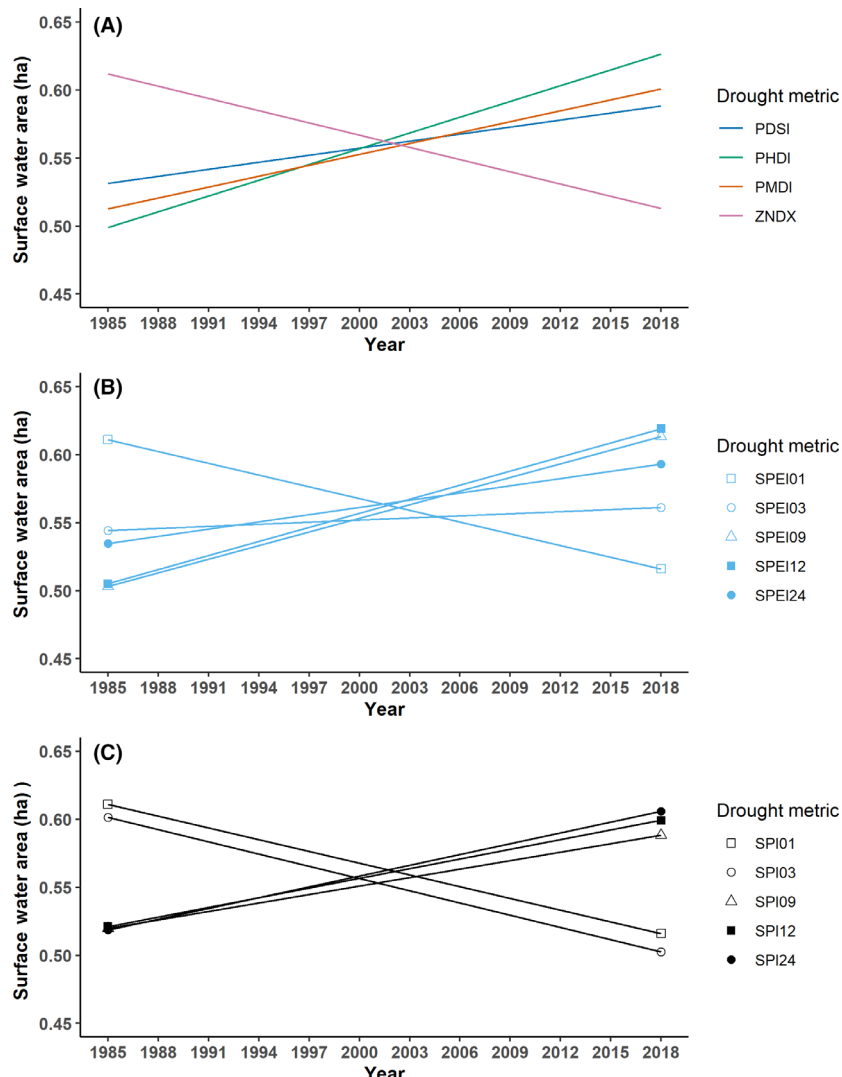


Figure 8. Predicted amount of surface water over time based on the estimated relationship between inundation extent and Palmer (A), SPEI (B), and SPI (C) drought indices and their respective durations (e.g. 12 vs 24 months) for all models fitted to the full dataset of 89 waterbodies (see Table 2).

followed by 9-months, 12-months, and 24-months. Surprisingly, models based on 1-month indices generally ranked similarly to 24-month models and had similar coefficients even though these indices were weakly

Table 4. Estimated changes (real scale) in surface area of waterbodies in the San Rafael Valley, Arizona, from September 1985 to September 2018

Model (3-mo SPI)	Annual rate (%) of change (95% CI)	Total per cent change (95% CI)
All waterbodies (N = 89)	0.42 (0.18–0.65)	13.86 (5.94–21.45)
Waterbodies ≤ 0.4 ha (N = 75)	0.40 (0.16–0.64)	14.52 (5.28–21.12)
25 most variable waterbodies	0.39 (0.00–0.78)	12.87 (0.00–26.07)

correlated themselves ($r \leq 0.30$; Appendix, Table S2). Estimated September surface water area was best described by a drought metric based on July–September precipitation, likely because most precipitation in our study area is channeled quickly into waterbodies from intense summer storms. Results from the Davis et al. (2019) study of wetlands dynamics in three regions of the USA were less consistent than ours, but they also found large differences in model support based on the number of months of data included in SPI indices, even for cases that differed by only 1 month (e.g. SPI02 vs. SPI03) or simply between seasons (fall vs. spring).

The effect of different drought indices and their durations was especially apparent when examining estimated changes in surface water over time. Based on analysis of all 89 sites or only the 75 sites ≤ 0.4 ha, only 4 of 14 fitted models—including the top-ranked SPI03 model—

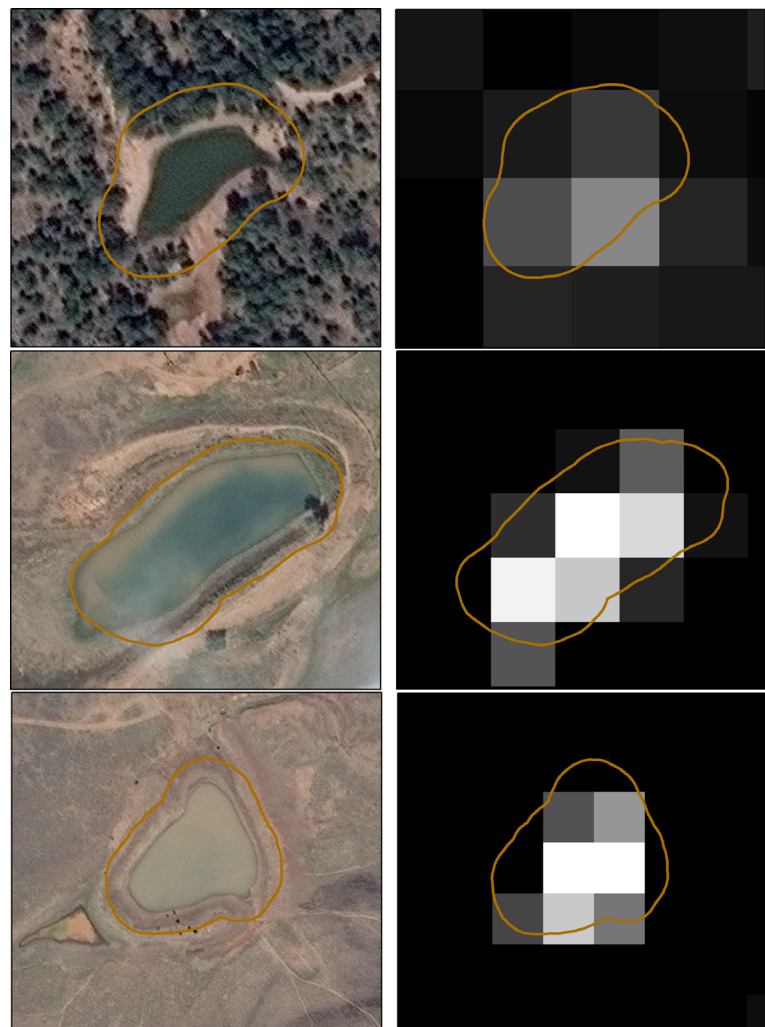


Figure 9. Example waterbodies from Landsat 8 validation image with different spectral characteristics (left: top to bottom, algae, turbid, mixed green-turbid) and corresponding matched filtering results (right).

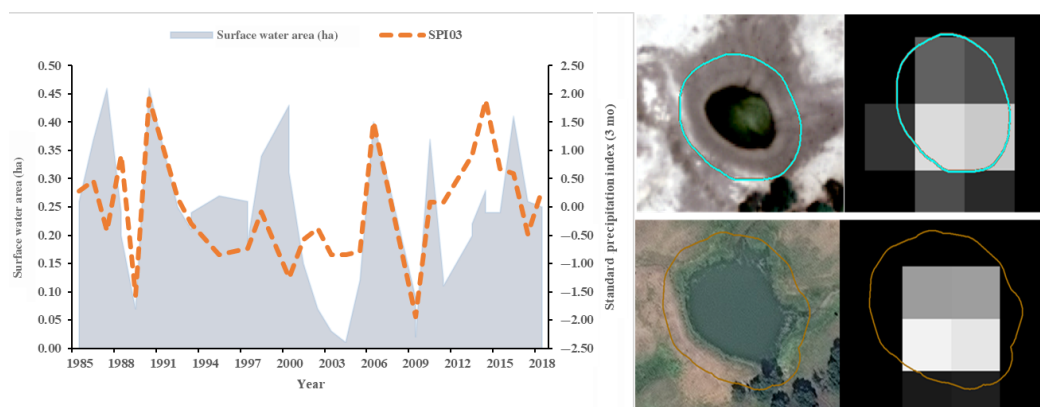


Figure 10. Example of a stock pond (Bog Hole Tank) that shrinks during dry seasons showing (left) annual variation in estimated inundation extent (September 1985–2018) and standard precipitation index (3 months) (top right) during June 2007 (digitized inundation extent 0.090 ha; modeled inundation extent 0.089 ha) and (bottom right) September 2018 (digitized inundation extent 0.275 ha; modeled inundation extent 0.235 ha).

estimated a decrease in surface water. The fitted SPI03 models for both datasets translated to an approximate 14% reduction in mean area of surface water from September 1985 to September 2018. When we estimated temporal trends in surface water for only the 25 waterbodies that varied most in size (based on CV; to help account for the presence of wells on some sites), all 14 models estimated a decrease in surface water over time. Although the smaller sample size and increased variation in this subset of 25 sites resulted in trend estimates that did not differ from zero, the estimated ~13% reduction in mean area of surface water was similar to that for the larger datasets; this suggests our results are robust. These decreases in surface water of small waterbodies since 1985 match declines in annual precipitation (Fig. 4) and are consistent with trends of observed and projected area of surface waters >0.09 ha across the south-western USA (Seager et al., 2013; Pekel et al., 2016).

Different system characteristics (e.g. stream flows and crop yields) can respond to drought on different timescales. Consequently, meteorological and hydrological indications of drought are not always closely coupled and can vary regionally (Vicente-Serrano et al., 2010; Bachmair et al., 2016). To more fully understand the potential threats to species that depend on these small waterbodies in the Southwest and other regions (e.g. Minckley et al., 2013; Hossack et al., 2017; Davis et al., 2019), it will be important to estimate long-term trends in surface water and the relationship with common drought indices during seasons when water is a more limited resource. It will also be important to assess the robustness of our methods for estimating surface water during dry seasons, when more sites would likely be very small, dry, or turbid and thus more challenging to measure accurately. Testing these methods in other study areas with waterbodies that have different features or are positioned differently in watersheds will be an important step toward extending these analyses beyond our study area. Collectively, the large differences in estimated amount of water on the landscape over time based on different drought indices and their durations in our study and others (e.g. Davis et al. 2019) emphasize the importance of understanding the local system when modeling past or future variation in surface water dynamics.

Acknowledgments

We thank G. Pederson and three anonymous reviewers for comments that improved this paper and for C. Crawford for facilitating access to some sites. Funding was provided by the U.S. Forest Service and the U.S. Geological Survey. This is contribution number 731 of the U.S. Geological Survey Amphibian Research and Monitoring

Initiative (ARMI). Any use of trade, firm, or product names is for descriptive purposes only and does not imply endorsement by the U.S. Government.

References

- Adams, D. K., and A. C. Comrie. 1997. The North American monsoon. *Bull. Amer. Meteor. Soc.* **78**, 2197–2214.
- Alley, W. M. 1984. The Palmer drought severity index: limitations and assumptions. *J. Clim. Appl. Meteor.* **23**, 1100–1109.
- Arizona Department of Water Resources. 2014. Climate of the San Rafael Basin. http://www.azwater.gov/AzDWR/Statewide_Planning/WaterAtlas/SEArizona/Climate/SanRafael.htm
- Bachmair, S., K. Stahl, K. Collins, J. Hannaford, M. Acreman, M. Svoboda, et al. 2016. Drought indicators revisited: the need for a wider consideration of environment and society: Drought indicators revisited. *WIREs Water* **3**, 516–536.
- Bates, D., M. Mächler, B. Bolker, and S. Walker. 2015. Fitting linear mixed-effects models using lme4. *J. Stat. Soft.* **67**, 1–48.
- Bishop-Taylor, R., S. Sagar, L. Lymburner, I. Alam, and J. Sixsmith. 2019. Sub-pixel waterline extraction: characterising accuracy and sensitivity to indices and spectra. *Remote Sens.* **11**, 2984.
- Brooks, R. T. 2005. A review of basin morphology and pool hydrology of isolated ponded wetlands: implications for seasonal forest pools of the northeastern United States. *Wetlands Ecol. Manage.* **13**, 335–348.
- Canals, R. M., V. Ferrer, A. Iriarte, S. Cárcamo, L. S. Emeterio, and E. Villanueva. 2011. Emerging conflicts for the environmental use of water in high-valuable rangelands. Can livestock water ponds be managed as artificial wetlands for amphibians? *Ecol. Eng.* **37**, 1443–1452.
- Carroll, M., and T. Loboda. 2017. Multi-decadal surface water dynamics in North American Tundra. *Remote Sens.* **9**, 497.
- Daly, C., M. Halbleib, J. I. Smith, W. P. Gibson, M. K. Doggett, G. H. Taylor, et al. 2008. Physiographically sensitive mapping of climatological temperature and precipitation across the conterminous United States. *Int. J. Climatol.* **28**, 2031–2064.
- Davis, C. L., D. A. W. Miller, E. H. Campbell Grant, B. J. Halstead, P. M. Kleeman, S. C. Walls, et al. 2019. Linking variability in climate to wetland habitat suitability: is it possible to forecast regional responses from simple climate measures? *Wetlands Ecol. Manage.* **27**, 39–53.
- DeVries, B., C. Huang, M. Lang, J. Jones, W. Huang, I. Creed, et al. 2017. Automated quantification of surface water inundation in wetlands using optical satellite imagery. *Remote Sens.* **9**, 807.
- Downing, J. A., Y. T. Prairie, J. J. Cole, C. M. Duarte, L. J. Tranvik, R. G. Striegl, et al. 2006. The global abundance and size distribution of lakes, ponds, and impoundments. *Limnol. Oceanogr.* **51**, 2388–2397.

- Frohn, R. C., E. D'Amico, C. Lane, B. Autrey, J. Rhodus, and H. Liu. 2012. Multi-temporal sub-pixel Landsat ETM+ classification of isolated wetlands in Cuyahoga County, Ohio, USA. *Wetlands* **32**, 289–299.
- Gallant, A. 2015. The challenges of remote monitoring of wetlands. *Remote Sens.* **7**, 10938–10950.
- Gibbs, J. P. 1993. Importance of small wetlands for the persistence of local populations of wetland-associated animals. *Wetlands* **13**, 25–31.
- Gilmore, S., A. Saleem, and A. Dewan. 2015. Effectiveness of DOS (Dark-Object Subtraction) method and water index techniques to map wetlands in a rapidly urbanising megacity with Landsat 8 data. *Research@ Locate'* **15**, 100–108.
- Greer, A. L., and J. P. Collins. 2008. Habitat fragmentation as a result of biotic and abiotic factors controls pathogen transmission throughout a host population. *J. Anim. Ecol.* **77**, 364–369.
- Guttman, N. B. 1998. Comparing the Palmer drought index and the standardized precipitation index. *J. Am. Water Resour. Assoc.* **34**, 113–121.
- Halabisky, M., L. M. Moskal, A. Gillespie, and M. Hannam. 2016. Reconstructing semi-arid wetland surface water dynamics through spectral mixture analysis of a time series of Landsat satellite images (1984–2011). *Remote Sens. Environ.* **177**, 171–183.
- Heddinghaus, T. R., and P. Sabol. 1991. A review of the palmer drought severity index and where do we go from here. Presented at the Proc. 7th Conf. on Applied Climatology, American Meteorological Society Boston, MA, pp. 242–246. <http://citeserx.ist.psu.edu/viewdoc/summary?doi=10.1.1.176.3020>; <http://citeserx.ist.psu.edu/viewdoc/download;jse ssionid=FE897A719A3DB6B5B78A156AA1944A1A?doi=10.1.1.176.3020&rep=rep1&type=pdf>
- Heinz, D. C., and Chang, C.-I. 2001. Fully constrained least squares linear spectral mixture analysis method for material quantification in hyperspectral imagery. *IEEE Trans. Geosci. Remote Sens.* **39**, 529–545.
- Hong, Z., X. Li, Y. Han, Y. Zhang, J. Wang, R. Zhou, et al. 2019. Automatic sub-pixel coastline extraction based on spectral mixture analysis using EO-1 Hyperion data. *Front. Earth Sci.* **13**, 478–494.
- Hossack, B. R., M. J. Adams, C. A. Pearl, K. W. Wilson, E. L. Bull, K. Lohr, et al. 2013. Roles of patch characteristics, drought frequency, and restoration in long-term trends of a widespread amphibian: regional drivers of amphibian trends. *Conserv. Biol.* **27**, 1410–1420.
- Hossack, B. R., R. K. Honeycutt, B. H. Sigafus, E. Muths, C. L. Crawford, T. R. Jones, et al. 2017. Informing recovery in a human-transformed landscape: drought-mediated coexistence alters population trends of an imperiled salamander and invasive predators. *Biol. Cons.* **209**, 377–394.
- Hu, Y. H., H. B. Lee, and F. L. Scarpace. 1999. Optimal linear spectral unmixing. *IEEE Trans. Geosci. Remote Sens.* **37**, 639–644.
- Huang, C., Y. Peng, M. Lang, I.-Y. Yeo, and G. McCarty. 2014. Wetland inundation mapping and change monitoring using Landsat and airborne LiDAR data. *Remote Sens. Environ.* **141**, 231–242.
- Ilori, C., N. Pahlevan, and A. Knudby. 2019. Analyzing performances of different atmospheric correction techniques for Landsat 8: application for coastal remote sensing. *Remote Sens.* **11**, 469.
- Jarchow, C. J., B. R. Hossack, B. H. Sigafus, C. R. Schwalbe, and E. Muths. 2016. Modeling habitat connectivity to inform reintroductions: a case study with the Chiricahua leopard frog. *J. Herpetol.* **50**, 63–69.
- Jarchow, C. J., B. H. Sigafus, E. Muths, and B. R. Hossack. 2019. Using full and partial unmixing algorithms to estimate the inundation extent of small, isolated stock ponds in an arid landscape. *Wetlands*. <https://doi.org/10.1007/s13157-019-01201-7>
- Jin, H., C. Huang, M. W. Lang, I.-Y. Yeo, and S. V. Stehman. 2017. Monitoring of wetland inundation dynamics in the Delmarva Peninsula using Landsat time-series imagery from 1985 to 2011. *Remote Sens. Environ.* **190**, 26–41.
- Jones, J. 2019. Improved automated detection of subpixel-scale inundation—revised Dynamic Surface Water Extent (DSWE) partial surface water tests. *Remote Sens.* **11**, 374.
- Karl, T. R. 1986. The sensitivity of the Palmer drought severity index and Palmer's Z-index to their calibration coefficients including potential evapotranspiration. *J. Clim. Appl. Meteor.* **25**, 77–86.
- Lake, P. S. 2003. Ecological effects of perturbation by drought in flowing waters. *Freshwater Biol.* **48**, 1161–1172.
- Li, L., Y. Chen, X. Yu, R. Liu, and C. Huang. 2015. Sub-pixel flood inundation mapping from multispectral remotely sensed images based on discrete particle swarm optimization. *ISPRS J. Photogramm. Remote Sens.* **101**, 10–21.
- Liu, X., R. Deng, J. Xu, and F. Zhang. 2017. Coupling the modified linear spectral mixture analysis and pixel-swapping methods for improving subpixel water mapping: application to the Pearl River Delta, China. *Water* **9**, 658.
- Minckley, T. A., D. S. Turner, and S. R. Weinstein. 2013. The relevance of wetland conservation in arid regions: A re-examination of vanishing communities in the American Southwest. *J. Arid Environ.* **88**, 213–221.
- Moses, W. J., S. Sterckx, M. J. Montes, L. De Keukelaere, and E. Knaeps. 2017. Atmospheric correction for inland waters. Pp. 69–100 in D. R. Mishra, I. Ogashawara, and A. A. Gitelson, eds. *Bio-optical modeling and remote sensing of inland waters*. Elsevier, Amsterdam. <https://doi.org/10.1016/B978-0-12-804644-9.00003-3>
- Palmer, W. C. 1965. *Meteorological drought*. U.S. Department of Commerce, Weather Bureau, Washington, DC. <https://www.ncdc.noaa.gov/temp-and-precip/drought/docs/palmer.pdf>

- Pekel, J.-F., A. Cottam, N. Gorelick, and A. S. Belward. 2016. High-resolution mapping of global surface water and its long-term changes. *Nature* **540**, 418–422.
- Rehage, J. S., S. E. Liston, K. J. Dunker, and W. F. Loftus. 2014. Fish community responses to the combined effects of decreased hydroperiod and nonnative fish invasions in a karst wetland: are everglades solution holes sinks for native fishes? *Wetlands* **34**, 159–173.
- Rover, J., B. K. Wylie, and L. Ji. 2010. A self-trained classification technique for producing 30 m percent-water maps from Landsat data. *Int. J. Remote Sens.* **31**, 2197–2203.
- Sakamoto, C. M. 1978. The Z-index as a variable for crop yield estimation. *Agric. Meteorol.* **19**, 305–313.
- Scheffer, M., G. J. van Geest, K. Zimmer, E. Jeppesen, M. Søndergaard, M. G. Butler, et al. 2006. Small habitat size and isolation can promote species richness: second-order effects on biodiversity in shallow lakes and ponds. *Oikos* **112**, 227–231.
- Seager, R., M. Ting, C. Li, N. Naik, B. Cook, J. Nakamura, et al. 2013. Projections of declining surface-water availability for the southwestern United States. *Nat. Clim. Change* **3**, 482–486.
- Tiner, R. W. 1990. Use of high-altitude aerial photography for inventorying forested wetlands in the United States. *For. Ecol. Manage.* **33–34**, 593–604.
- Torbick, N., S. Hession, S. Hagen, N. Wiangwang, B. Becker, and J. Qi. 2013. Mapping inland lake water quality across the Lower Peninsula of Michigan using Landsat TM imagery. *Int. J. Remote Sens.* **34**, 7607–7624.
- Tulbure, M. G., and M. Broich. 2013. Spatiotemporal dynamic of surface water bodies using Landsat time-series data from 1999 to 2011. *ISPRS J. Photogramm. Remote Sens.* **79**, 44–52.
- Vicente-Serrano, S. M., S. Beguería, and J. I. López-Moreno. 2010. A multiscalar drought index sensitive to global warming: the standardized precipitation evapotranspiration index. *J. Climate* **23**, 1696–1718.
- Vicente-Serrano, S. M., S. Beguería, J. Lorenzo-Lacruz, J. J. Camarero, J. I. López-Moreno, C. Azorin-Molina, et al. 2012. Performance of drought indices for ecological, agricultural, and hydrological applications. *Earth Interact.* **16**, 1–27.
- Vose, R. S., S. Applequist, M. Squires, I. Durre, M. J. Menne, C. N. Williams, et al. 2014. Improved historical temperature and precipitation time series for U.S. climate divisions. *J. Appl. Meteor. Climatol.* **53**, 1232–1251.
- Walls, S. C., W. J. Barichivich, M. E. Brown, D. E. Scott, and B. R. Hossack. 2013. Influence of drought on salamander occupancy of isolated wetlands on the southeastern coastal plain of the United States. *Wetlands* **33**, 345–354.
- Williams, P., M. Whitfield, J. Biggs, S. Bray, G. Fox, P. Nicolet, et al. 2003. Comparative biodiversity of rivers, streams, ditches and ponds in an agricultural landscape in Southern England. *Biol. Cons.* **115**, 329–341.
- Zhao, D., P. Wang, J. Zuo, H. Zhang, S. An, and R. K. Ramesh. 2017. Are the traditional large-scale drought indices suitable for shallow water wetlands? An example in the Everglades. *J. Environ. Manage.* **198**, 240–247.

Supporting Information

Additional supporting information may be found online in the Supporting Information section at the end of the article.

Table S1. Landsat imagery used to validate the surface water extent predictions from matched filtering using two references data.

Table S2. Correlation matrix (Pearson's r) of the association among annual precipitation (ANNPPT; Oct–Sep) and the different drought indices we used. All drought indices were indexed to September.